Simultaneous Aircraft Sizing and Multi-Objective Optimization Considering Off-Design Mission Performance during Early Design

Abstract

Traditional aircraft conceptual design primarily involves determination of top-level sizing parameters, resulting in an initial design which satisfies specified point-performance constraints while flying the so-called design mission. In practical scenarios, commercial aircraft are also expected to operate optimally in the actual missions they fly which may drastically differ from the design mission. To improve performance and reduce operating costs, optimization shall be performed using specific objectives from the on-design mission and from one or more representative off-design reference mission(s). Such multi-mission optimizations may result in different designs for the same performance constraints. Moreover, the size of aircraft and choice of reference mission(s) may also have an effect in the difference resulting from such multi-mission optimizations. This paper solves a series of multi-objective on-design and multi-mission optimization problems in the conceptual design phase on aircraft spanning a range of size-classes, using the Non-dominated Sorting Genetic Algorithm II (NSGA-II). Results shed light on the design differences between formulations that exclusively consider design mission metrics of interest from the ones that consider metrics of interest from disparate, as-flown, i.e., off-design missions. In addition, results also reveal the impact of off-design mission weightings on the designs obtained from the optimization problems.

Keywords: Conceptual Design, Commercial Aircraft Sizing, Off-design Optimization, Multi-objective Optimization, Payload-range Characteristics

1. Introduction

The primary goal of aircraft sizing in conceptual design phase is to use point performance and mission performance requirements to obtain an initial estimate of the geometric scale, the propulsion characteristics, and the design gross weight, which are typically represented by the wing planform area, the rated sea-level static thrust, and the maximum takeoff weight, (MTOW), respectively. Traditionally, this process yields a solution which satisfies the performance requirements for the so-called design mission. Due to airlines' concerns with regard to operating and maintenance costs and environmental factors such as noise and emissions, the design is optimized for objectives such as MTOW, operating empty weight (OEW), takeoff field length (TOFL), noise, and/or fuel consumption of the mission for which the aircraft is sized, i.e., the design mission.

While commercial aircraft are sized to fly the design mission, in real-world operations, the aircraft operate a variety of off-design missions with diverse payload and range combinations. In some cases, airlines sacrifice payload capacity in order to fly certain ultra-long-range missions. For example, Singapore Airlines used to operate non-stop flights between Singapore and New York at a great circle distance of 8300 nmi using the Airbus A340-500 aircraft in a special configuration carrying only 100 passengers instead of the typical 293-seat configuration [1]. In other cases, many airlines operate long-range aircraft on much shorter routes due to airport slot constraints, capacity demand, and/or fleet utility, etc. For example, the long-range Airbus A350, A380, Boeing 787, and 777 are frequently used on short-haul high-capacity flights within Asia.

From the airlines' perspective, design optimization considering off-design performance offers the prospect of high mission flexibility along with the promise of operating the actual missions as efficiently as possible. This can be achieved by choosing off-design metrics such as specific air range (SAR) instead of the design mission performance such as the block fuel (BF). However, one, such formulations may not shed light on whether and if so, how the choice of objective mission performance metric impacts the payload-range capability and performance of other off-design missions under identical point performance and design mission requirements; two, the distribution of off-design missions relative to the design mission in the payload-range space may also affect the trade-off (if present) mentioned above.

The primary goal of this work is to investigate the aforementioned issues through several multi-mission multi-objective sizing and optimization studies to assess the differences in top-level aircraft design parameters and off-design mission performance metrics among the Pareto optimal designs across a few size-classes, specifically, a Regional Jet (RJ), a Small Single-aisle Aircraft (SSA), and a Large Twin-aisle Aircraft (LTA).

Researchers have attempted off-design optimization using a single-objective or "a-priori" multi-objective optimization problem formulations [2, 3, 4, 5, 6], where multiple objectives were aggregated into a single objective function by defining a "utility function" or "value function" instead of investigating a set of Pareto optimal solutions. A-posteriori multi-objective optimization problem formulations have also been leveraged [7, 8, 9, 10] to obtain Pareto frontiers to investigate the trade-off between aircraft gross weight, design mission fuel burn, noise, and emissions, etc., but these studies do not explicitly factor-in off-design considerations. This work, on the other hand, highlights the insights gained from a multi-mission a-posteriori multi-objective optimization performed on both on-design and off-design mission performance metrics.

The appropriate size of an aircraft's design parametrization is a largely neglected issue in aircraft conceptual design and optimization studies. Typically, the extent of parametrization is constrained by both the lack of information and the semi-empirical nature of the component weight build-up, aerodynamics, and propulsion models. Notable studies [3, 4, 5, 6, 8, 9, 10] on aircraft sizing and optimization decide the number of parameters describing an aircraft based on either a widely accepted set of significant inputs and subject matter expertise, or by considering all the variables availed by their respective analysis tools. It is a well-recognized and widely accepted fact that a majority of the metrics of interest in conceptual design are largely affected by a few key scaling factors such as the geometric and the propulsive scale, i.e., the wing loading and thrust loading respectively. However, other geometric aircraft parameters cannot simply be neglected because they may have significant secondary effects on the metrics of interest through their appearance in equations for component weight build-ups which affect the weight, and therefore, the aerodynamics and propulsion characteristics. On the other hand, considering all the possible parameters exposed by respective analyses may introduce variables that affect the outputs insignificantly. Consequently, including such variables leads to relatively complex and hard-to-solve optimization problem formulations while only adding marginal value. Moreover, the effect of input variables on the metrics of interest also depends on the fidelity of the underlying analysis. To address the aforementioned issues, this work proposes beginning with the full set of relevant inputs and down-selecting the most important ones for the specific metrics of interest by rank-ordering them based on the significance of their effect on the outputs. Such a screening procedure ensures a parsimonious optimization problem while ensuring that a majority of the variation in the outputs is retained.

The primary goal of this work is accomplished by proposing and leveraging a methodology that: one, formulates and compares the insights from on-design and off-design optimization problems. A practically meaningful off-design optimization problem is constructed by performing a thorough assessment of several off-design objective functions and identifying conflicting ones; two, provides a principled method to construct a parsimonious optimization problem by down-selecting the most significant inputs via sensitivity analysis, considering an exhaustive set of conceptual phase aircraft design parameters. The developed methodology is design tool agnostic and is easily extensible to a wide range of aircraft concepts and mission types. The salient novel features of the study are: 1) both on-design and off-design quantities of interest are considered in the a-posteriori multi-objective optimization setting, 2) a thorough study, with a large set of design variables, is performed across major aircraft size classes to give an insight into the trade-offs involved within them with regard to on-design and off-design considerations.

The remainder of this paper is organized as follows: Sec. 2 presents the formulation of both the on-design and off-design optimization problems; Sec. 3 discusses the methods used in major disciplinary analyses performed in conceptual aircraft design; Sec. 4 describes the mission profile and the tool to perform off-design mission performance evaluation; Sec. 5 briefly describes the characteristics of NSGA-II, the optimization algorithm used in this paper; Sec. 6 presents the optimization results along with discussions; finally, Sec. 7 draws the conclusion.

2. Problem Formulation

This section describes the objectives considered for the on-design (single-mission) optimization and the off-design (multi-mission) optimization in Sec. 2.1, the constraints considered for both optimization problems in Sec. 2.2, the set of aircraft-level design variables in Sec. 2.3, the necessity for down-selecting the design variables through screening in Sec. 2.4, the complete problem statement in Sec. 2.5, and finally, the reference vehicles' data and the corresponding design variable ranges in Sec. 2.6.

2.1. Objective Functions

The problem of optimizing the performance of an aircraft for multiple missions simultaneously while sizing the aircraft for a single design mission is naturally posed as a multi-objective optimization problem. In the literature concerning aircraft design optimization at the conceptual stage, researchers have considered a number of objective functions motivated mainly by the intended objectives of the specific study [8, 11]. Because the goal of this work is to compare differences in designs when on-design and off-design metrics are taken into account together, formulations with a mix of mission-invariant and mission-dependent metrics are considered. The mission-invariant metrics imply the capability of a sized aircraft, regardless of the actual mission being operated, whereas the mission-dependent metrics measure the performance of a sized aircraft which depends on the actual mission being flown.

For the on-design optimization, two mission-invariant objectives are considered: 1) the maximum ramp weight, MRW, and 2) the nominal takeoff field length, TOFL, computed at standard sea level conditions and at maximum takeoff weight. A third objective for the on-design optimization is the block fuel of the design mission, $W_{BF,des}$, which is a good measurement of the direct operating cost when the aircraft flies the design mission.

For the off-design optimization, the on-design objectives to minimize MRW and TOFL remain. A third objective to be minimized is selected among the following three candidate functions involving mission-dependent variables, i.e. functions of payload (W_P) and range (R):

$$O_1 = \iint_M f(W_P, R)\; W_{BF}(W_P, R)\, dW_P\, dR \tag{1}$$

$$O_2 = -\iint_M f(W_P, R)\; \frac{R}{W_{BF}(W_P, R)}\, dW_P\, dR \tag{2}$$

$$O_3 = -\iint_M f(W_P, R)\; \frac{W_P R}{W_{BF}(W_P, R)}\, dW_P\, dR \tag{3}$$

where M represents the feasible mission space as dictated by a domain bounded by the maximum takeoff weight, maximum fuel capacity, and maximum payload weight constraints in mission range and payload space for a sized vehicle; $f(W_P, R)$ is a weighting function for the off-design missions, and to serve its purpose, this work chooses the mission frequency distribution function, i.e. normalized frequency or expected probability density that an aircraft of a single type will operate the mission specified by a given payload and range combination; finally, W_{BF} is the mission-dependent block fuel which is assumed to depend solely on payload and still-air range for a sized aircraft. Before proceeding, listed below are some noteworthy points regarding the three candidate off-design objectives mentioned above:

- In O_1, the mission block fuel W_{BF} directly relates to fuel cost, which is the most significant contributor to the operating cost

- In O_2, the term R/W_{BF} is the mission-averaged specific air range, an indicator of fuel efficiency for a given mission
- In O_3, the term $W_P R$ is a good representative for airline revenue when carrying the payload of W_P over a distance of R; the fraction $W_P R/W_{BF}$ measures the flight productivity for a given mission

From the operators' perspective, the flight productivity is of most interest among the three discussed, simply because it meaningfully combines payload, range, and fuel consumption simultaneously. Similar to O_3, Hileman et al. [12] proposed a metric named payload fuel energy efficiency (PFEE) as a measure of flight productivity. For a single mission, PFEE is defined as [12]

$$\text{PFEE} = \frac{\text{Total payload carried} \times \text{Great-circle distance}}{\text{Fuel energy consumed}} \tag{4}$$

This work adopts the original definition of PFEE and modifies it based on the goal of the optimization problem in question. For the on-design optimization, minimizing the block fuel of the design mission is equivalent to minimizing the negative on-design PFEE, defined as

$$-\text{PFEE}_0 = -\frac{W_{P,des} R_{des}}{W_{BF,des} q_{fuel}/g} \tag{5}$$

where g is the gravitational acceleration and $q_{fuel} = 42.80\,\text{MJ/kg}$ is the specific energy of Jet-A fuel [13], which essentially serves as a normalization factor to non-dimensionalize the metric. For the off-design optimization, the third objective to minimize is the negative average off-design PFEE, defined as

$$-\text{PFEE}_1 = -\iint_M f(W_P, R)\, \frac{W_P R}{W_{BF}(W_P, R) q_{fuel}/g}\, dW_P\, dR \tag{6}$$

Besides the flight productivity implied by PFEE_1, another metric to consider in the off-design scenario is the mission coverage index (MCI), defined as the cumulative mission frequency or mission probability density within the payload-range envelope of a sized vehicle. MCI must be regarded as an important metric since potential aircraft customers may have specific requirements on the payload and range capability of the aircraft. Note that large MCI values imply that the aircraft can optimally operate for larger number of payload-range combinations within the envelope for a prescribed mission frequency distribution. In certain cases, a higher MCI can only be achievable by up-sizing the aircraft, i.e. increasing the MRW and/or design fuel capacity, which is accompanied by an increase in the operating empty weight, an overall increase in fuel consumption within the payload-range envelope, and a decrease in PFEE_1. Therefore, MCI and PFEE_1 are conflicting in nature, implying the existence of a Pareto frontier when optimized simultaneously. In this work, the negative MCI is included as the fourth and last objective to be minimized for the off-design optimization, as shown in Eq. (7):

$$-\mathrm{MCI} = -\iint_M f(W_P, R)\, dW_P\, dR \tag{7}$$

2.2. Constraint Functions

The optimization problem statement is subject to performance, regulatory, and operational constraints, each of which is cast as a nonlinear inequality constraint. A total of five constraints are considered in this work: the positive second segment climb thrust (SSFOR) and positive missed approach gradient thrust (AMFOR) constraints [14] place lower bounds on permissible thrust-to-weight ratio; the upper-bound on permissible landing approach speed (VAPP) constrains the maximum feasible wing loading; the upper-bound on wingspan (SPAN) constrains the feasible wing aspect ratio given a wing area; and the upper-bound on vertical tail height (VTH) constrains the feasible vertical tail aspect ratio for a given vertical tail area, which is governed by the wing geometry through constant vertical tail volume coefficient. Finally, the bounds for VAPP, SPAN, and VTH are determined based on the specifications of FAA Aircraft Design Category [15].

2.3. Design Variables and Bounds

As mentioned in Sec. 1, any trade-off in terms of optimality is expected to be revealed by using a combination of both on-design and off-design metrics. Accessibility to designers and an ability to significantly impact the aerodynamics, propulsion, and weights disciplines motivate the choice of design variables in the conceptual phase.

The thrust-to-weight ratio (TWR) and the wing loading (WSR) are scaling parameters that affect top-level aircraft point performance such as takeoff field length, approach speed, rate of climb, etc. [16] The wing and tailplane geometries are expected to have significant impact on component weights and aerodynamic characteristics, therefore affecting the vehicle gross weight, performance, and fuel consumption. Consequently, this work considers the aspect ratio, taper ratio, average thickness-to-chord ratio, and quarter-chord sweep angle of the wing, the horizontal tail, and the vertical tail as the geometric design variables. To maintain invariant stability and control characteristics when sizing the vehicle for different design variables, the tail volume coefficients are held constant.

TWR, WSR, and the geometric design variables are continuous variables, which may take any value within defined upper and lower bounds. Typical ranges for the design variables are chosen such that the resulting aircraft remains within its size-class. Given a baseline vehicle in a certain size-class, this work uses a $\pm 10\%$ variation about the baseline values for TWR, WSR, aspect ratios, taper ratios, and thickness-to-chord ratios, a $\pm 5\,\text{deg}$ variation for wing sweep angle, and a $\pm 10\,\text{deg}$ variation for tail sweep angles.

In traditional on-design aircraft sizing methods, the design mission is often regarded as an equality constraint, i.e. the aircraft is sized to have a range capability of exactly the design range when carrying the design payload. However, in the case of off-design optimization, depending on the distribution of mission weighting function $f(W_P, R)$ and the relative location of design mission $(W_{P,des}, R_{des})$ in the mission space, it may be necessary to up-size the vehicle such that its feasible mission space M covers a larger region where

$f(W_P, R) > 0$, thus potentially increasing PFEE_1 and/or MC. In this study, an increase in the aircraft's range capability when carrying the design payload is chosen to represent the up-sizing. Therefore, the design range capability (DESRNG) is included as the final design variable with only a lower bound constraint equal to the required design range (R_{des}).

A summary of the design variables and their bounds relative to the reference vehicles (to be discussed in Sec. 2.6) is presented in Table 1.

Table 1: Design Variables and Bounds Relative to Baseline Values

Group	Design Variable	Min	Max
Vehicle-level parameters	Design range capability, DESRNG	$+0\%$	∞
	Thrust-to-weight ratio, TWR	-10%	$+10\%$
	Wing loading, WSR	-10%	$+10\%$
Wing geometry	Aspect ratio, AR	-10%	$+10\%$
	Taper ratio, TR	-10%	$+10\%$
	Thickness-to-chord ratio, TCA	-10%	$+10\%$
	Quarter-chord sweep angle, SWEEP	$-5°$	$+5°$
Horizontal tail geometry	Aspect ratio, ARHT	-10%	$+10\%$
	Taper ratio, TRHT	-10%	$+10\%$
	Thickness-to-chord ratio, TCHT	-10%	$+10\%$
	Quarter-chord sweep angle, SWPHT	$-10°$	$+10°$
Vertical tail geometry	Aspect ratio, ARVT	-10%	$+10\%$
	Taper ratio, TRVT	-10%	$+10\%$
	Thickness-to-chord ratio, TCVT	-10%	$+10\%$
	Quarter-chord sweep angle, SWPVT	$-10°$	$+10°$

2.4. Design Space Reduction via Sensitivity Analysis

Several challenges need to be tackled especially when performing many-query exercises with computationally expensive, black-box functions in high-dimensional parameter spaces. Wang et al. [17, 18] classify techniques to reduce the input space dimensionality in the context of surrogate modeling into decomposition-, mapping-, screening-, and visualization-based approaches.

Decomposition-based techniques partition the original problem into smaller, more manageable sub-problems; the choice of decomposition is often subjective, when and if a given problem is decomposable. The goal of mapping-based approaches is to find a transformation that maps a set of correlated variables into a new, smaller set of uncorrelated variables that retain most of the original information. While mapping aids both optimization and modeling by alleviating the *curse of dimensionality*, the optimization must occur in the low dimensional space. Moreover, it must be assumed that a mapping from the low dimensional space to the original high dimensional space exists and lies within the feasible design space. While these challenges can be tackled, this work relies on a simpler screening-based approach to manage the size of the input space.

Screening methods reduce dimensionality by exploiting sampled points to recognize and retain the most important inputs and their interactions while removing noise and other insignificant contributors to variability in the outputs. Analysis of variance [19], weighted average of local sensitivity, partial rank correlation coefficient, multi-parametric sensitivity analysis, and Fourier amplitude sensitivity analysis and Sobol's [20] method are common techniques to perform screening. Once the significant variables and interactions are identified, the other variables are either simply dropped from consideration (for instance, in the case of surrogate modeling), or held constant at some nominal baseline value (for instance, in the case of optimization). In multi-objective optimization, fixing the insignificant contributors to nominal baseline values allows for an easier-to-solve optimization problem at the cost of convergence to a marginally different Pareto optimal set.

In this work, the most important set of inputs for formulating the optimization problem is chosen using Sobol's [20] method; a global sensitivity analysis approach which decomposes a model output's variance into summands of variances of the input parameters to determine the contribution of each input and their interactions. The set of objectives and constraints is first evaluated for the set of optimal experiments generated using Saltelli's sampling scheme [21] using the aircraft sizing and mission analysis code (described in Sec. 4) Then, the Sobol's method is applied to each objective and constraint function independently to determine the effective set of input variables to capture a prescribed normalized output variance threshold. Finally, the optimization problem is formulated by considering the inputs obtained by taking a superset of significant contributors to each objective and constraint function.

2.5. Formal Optimization Problem

Considering the objective functions, constraints, and design variables described earlier, the on-design and off-design optimization problems may now be formally stated as

$$
\begin{aligned}
\underset{\mathbf{x}}{\text{minimize}} \quad & \mathbf{f}(\mathbf{x}) = \begin{bmatrix} \mathrm{MRW}(\mathbf{x}) \\ \mathrm{TOFL}(\mathbf{x}) \\ -\mathrm{PFEE}_0(\mathbf{x}) \end{bmatrix} \quad \text{or} \quad \mathbf{g}(\mathbf{x}) = \begin{bmatrix} \mathrm{MRW}(\mathbf{x}) \\ \mathrm{TOFL}(\mathbf{x}) \\ -\mathrm{PFEE}_1(\mathbf{x}) \\ -\mathrm{MCI}(\mathbf{x}) \end{bmatrix} \\
\text{subject to} \quad & \mathrm{SPAN}(\mathbf{x}) - \mathrm{SPAN}_{\max} \leq 0, \\
& \mathrm{VTH}(\mathbf{x}) - \mathrm{VTH}_{\max} \leq 0, \\
& \mathrm{VAPP}(\mathbf{x}) - \mathrm{VAPP}_{\max} \leq 0, \\
& -\mathrm{AMFOR}(\mathbf{x}) \leq 0, \\
& -\mathrm{SSFOR}(\mathbf{x}) \leq 0, \\
& \mathbf{x} : [\text{Effective Design Variables}] \in [\text{Table 1 intervals}]
\end{aligned}
$$

where $\mathbf{f}(\mathbf{x})$ and $\mathbf{g}(\mathbf{x})$ are the on-design and off-design objectives, respectively, and the set of effective design variables is determined with the following steps:

1. Perform screening tests on each objective and constraint considered;
2. Given a threshold between 0 and 100%, for each response, identify the minimal set of design variables which captures a cumulative percentage total variation greater than the threshold;

3. The final set of effective design variables is chosen as the superset of all sets identified in step 2.

2.6. Aircraft Size-Classes Considered and Reference Vehicles

This work considers the assessment of three aircraft size-classes, each represented by a Regional Jet (RJ), a Small Single-aisle Aircraft (SSA), and a Large Twin-aisle Aircraft (LTA), respectively. The RJ has a T-tail and tail-mounted nacelle configuration, whereas the SSA and LTA have a conventional tail and under-wing nacelle configuration. The baseline aircraft specifications are shown in Table 2 and the constraints for each size-class are presented in Table 3. The mission frequency distribution function $f(W_P, R)$ is obtained by collecting data from the U.S. Department of Transportation Bureau of Transportation Statistics Form 41 Schedule T-2 database [22]. Data on passenger-carrying flights between January 2014 and September 2018 for the Bombardier CRJ900, Boeing 737-800, and Boeing 777-200 (all variants) are used to represent the mission frequency distribution of the RJ, SSA, and LTA size-classes, respectively. Before proceeding, the readers must be cautioned about the following caveats:

- The historical data only include flights departing from and/or arriving in the United States, thus merely serving as examples of potential representative mission distributions for this work. By no means are they intended to represent actual worldwide operations.

- The reported flight distance in the database is the great circle distance between the origin and the destination airports. The actual still-air flight distance depends on routing and en-route wind considerations, which is unique to each flight. In this work, the reported flight distance is divided by an average horizontal flight efficiency of 0.93 [23] in order to obtain an estimate of still air distance to be used in off-design mission analysis.

Table 2: Baseline aircraft specifications

Parameter	**RJ**	**SSA**	**LTA**
Thrust-to-weight ratio	0.338	0.312	0.296
Wing loading, lb/ft^2	113	124.1	133.3
Passenger capacity	86	160	305
Design payload weight, lb	17 200	33 600	64 050
Design range, nmi	1900	2900	7500
Cruise Mach number	0.780	0.785	0.840
Maximum cruise altitude, ft	41 000	41 000	43 000
Maximum payload weight, lb	22 750	47 000	125 500
Wing quarter-chord sweep, deg	27.0	25.7	30.9
Wing aspect ratio	8.29	9.74	8.81
Wing taper ratio	0.281	0.312	0.176
Wing thickness-to-chord ratio	0.109	0.109	0.109
Horizontal tail quarter-chord sweep, deg	29.5	29.9	34.8
Horizontal tail aspect ratio	4.59	6.27	4.62
Horizontal tail taper ratio	0.461	0.203	0.330
Horizontal tail thickness-to-chord ratio	0.094	0.109	0.088
Vertical tail quarter-chord sweep, deg	43.2	35.0	40.0
Vertical tail aspect ratio	1.11	1.92	1.84
Vertical tail taper ratio	0.644	0.276	0.299
Vertical tail thickness-to-chord ratio	0.110	0.115	0.093

Table 3: Size-dependent constraints for the RJ, SSA, and LTA size-classes

Constraint	**RJ**	**SSA**	**LTA**
FAA Design Category	C-II	C-III	D-V
SPAN_{max} (ft)	79	118	214
VTH_{max} (ft)	30	45	66
VAPP_{max} (kts)	140	140	165

3. Major Disciplinary Analyses in Conceptual Aircraft Design

The aircraft design process is multidisciplinary in nature due to the inherent complexity of an aircraft as a system. Figure 1 lists a few major disciplines that play a significant role at various different stages in the aircraft design process. Due to the uneven distribution of knowledge throughout the aircraft design process [24], emphases are primarily placed on aerodynamic analysis, weight estimation, and preliminary propulsion system sizing in conceptual design stage.

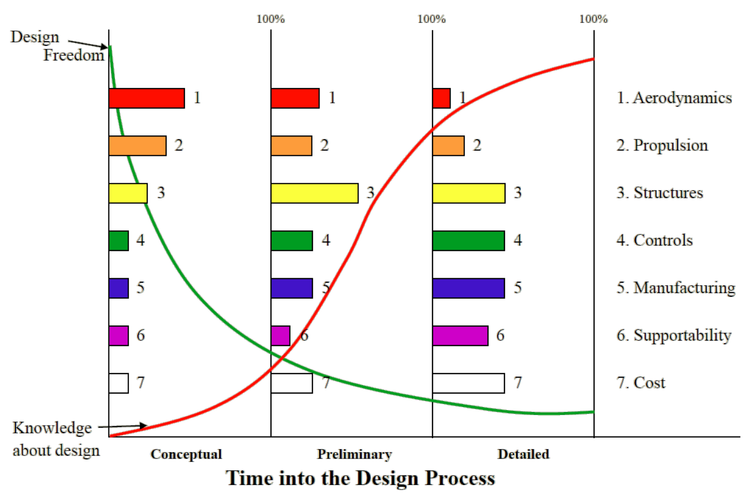

Figure 1: Uneven distribution of knowledge in the aircraft design process [24]

3.1. Aerodynamics Analysis

The aerodynamic characteristics are estimated using the semi-empirical drag build-up method used by NASA software Flight Optimization System (FLOPS) [25]. FLOPS internally computes the drag of wing, empennage, fuselage, nacelles, and other miscellaneous elements dynamically as the size of the components changes during sizing iterations. The aircraft drag coefficient is assumed to be a function of flight altitude, Mach number, and aircraft lift coefficient.

3.2. Weights Estimation

In conceptual design, aircraft empty weight estimation typically employs semi-empirical regression-based methods rather than fully physics-based methods due to the need for rapid design space exploration, which requires evaluation of a large amount of design candidates with limited computational resources and time [26]. Existing regression-based methods include the Raymer method [27], the Roskam method [28], and the FLOPS method [29], all of which compute the weight of each component and take their sum to obtain the aircraft empty weight. In this paper, the FLOPS method is used for weight estimation, where the component weights are dynamically computed based primarily on geometric parameters, rated thrust, and extreme flight conditions with the assumption that a conventional subsystem architecture is installed in the aircraft.

3.3. Propulsion System Scaling

The engine model of each baseline aircraft is sized using Numerical Propulsion System Simulation (NPSS) [30] such that the rated thrust matches the sea level static thrust based on the baseline design gross weight and thrust-to-weight ratio. NPSS also generates an engine deck containing the variation of thrust and fuel flow as functions of Mach number, altitude, and power code (a surrogate for the throttle setting). The baseline engine weight and dimensions are computed using the Object-Oriented Weight Analysis of Turbine Engines computer code (WATE++) [31]. For a design candidate, if the desired rated thrust is different from that of the baseline engine, the engine weight and dimensions are scaled using the FLOPS method [29]. The thrust specific fuel consumption as a function of power code, altitude, and Mach number of the scaled engine is assumed to be identical to that of the baseline engine. The drag of the scaled engine nacelles is recalculated in FLOPS based on the actual dimensions.

4. Mission Analysis

4.1. Mission Profile and Fuel Requirements

A generic commercial transport mission profile, as shown in Fig. 2, is assumed for all missions studied in this work. This work assumes a generic commercial transport mission profile, as shown in Fig. 2, for all the missions considered. All climb segments use a minimum fuel-to-climb profile and the cruise segments of the regular mission are flown at a constant design Mach number as specified in Table 2. Actual missions operated by commercial aircraft are simulated by assuming that a step cruise is performed at the design Mach number at altitudes between 29 000 ft and the service ceiling with an increment of 2000 ft, based on the rules of Reduced Vertical Separation Minimum (RVSM) [32]. Between the altitudes mentioned above, the specific air range (SAR) is maximized to obtain the initial cruise altitude, i.e., the altitude at which the aircraft begins its cruise segment. The aircraft climbs to the next available higher altitude if the SAR at the new altitude is larger (due to a decrease in the gross weight) than the current SAR. As an additional requirement, the aircraft is constrained to perform a step climb in the last step cruise segment before descending only if a minimum remaining cruise distance of 300 nmi is available. The descent segment is flown at the optimum lift-to-drag ratio. The reserve mission consists of a missed approach, followed by a climb to the reserve altitude, a cruise segment at the optimum Mach number for SAR, a descent to 1500 ft, and a hold (loiter) for 30 min at the optimum Mach number for endurance.

As shown in Fig. 2, the mission fuel is defined as the required amount of fuel on-board at the start of the mission, including both the block fuel and the reserve fuel. The block fuel is the amount of fuel consumed between engine start

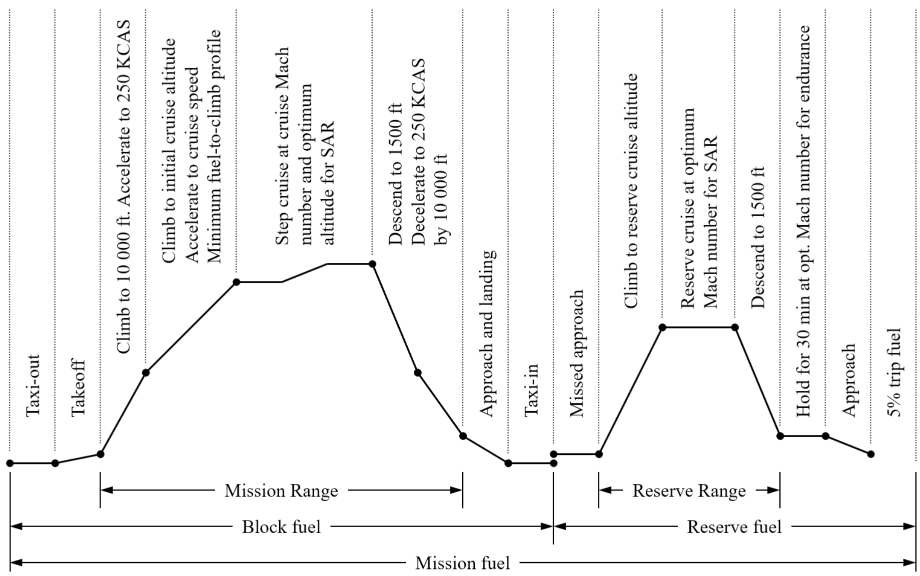

Figure 2: Generic mission profile for commercial aircraft

and engine shutdown for a regular mission. The reserve fuel includes the fuel required to fly the reserve mission, plus an additional 5 % on top of the regular and the reserve mission fuel.

For the vehicles considered in this work, fuel is assumed to be stored entirely in wing fuel tanks, including wing center fuel tanks, without fuselage tanks. The wing fuel tank volume is estimated and scaled based on wing geometric parameters in the FLOPS method [29], as shown in Eq. (8):

$$V_{wt} = k_{wt} z_t \frac{S_w^2}{b} \left(1 - \frac{\lambda}{(1+\lambda)^2}\right) \tag{8}$$

where k_{wt} is a non-dimensional tank volume coefficient, S_w is the wing planform area, z_t is the wing average thickness-to-chord ratio (equivalent to TCA), b is the wingspan (equivalent to SPAN), and λ is the wing taper ratio (equivalent TR). The value of k_{wt} for each size-class is calibrated based on the corresponding baseline aircraft in Table 2, and is held invariant during sizing for all design candidates of that size-class.

4.2. Mission Performance Evaluation with Gross Weight and Fuel Capacity Constraints

The mission performance is evaluated in FLOPS, which accepts climb, cruise, and descent schedule definitions as inputs, and performs internal optimization to find the optimum vertical trajectory satisfying the mission profile described in Sec. 4.1, subject to the constraints of gross weight, zero fuel weight, and mission range [25].

Traditionally, when a design candidate is being sized and the design mission is being evaluated, the mission analysis assumes that the aircraft departs at the same gross weight used to scale the geometry and the engines and to perform weight estimation [27, 16], which is typically referred to as the maximum ramp weight (MRW). This approach implicitly assumes that the difference between the MRW and the zero fuel weight (sum of operating empty weight and payload weight) is the weight of available fuel which can be achieved by filling the fuel tanks; the resulting payload-range envelope is expected to be similar to Fig. 3(a).

However, such an assumption does not always hold true. When a vehicle is to be sized for a relatively high design wing loading (WSR), it is likely that the fuel tanks in the small wing would fail to contain the fuel required for the design mission, thus invalidating the resulting design even if the vehicle sizing converges, as shown in Fig. 3(b). In this case, the design mission is *fuel-constrained* instead of being *weight-constrained*.

To address this gap, in this work, a local optimizer is added to the existing mission analysis. The vehicle size is iteratively adjusted, meaning that a new value of MRW is assigned, followed by re-evaluation of geometry (including fuel tank capacity), aerodynamic characteristics, component weights, and engine scaling, while TWR and WSR are held constant. The mission analysis is then repeated to obtain the updated fuel requirement for the design mission. The optimization converges when the fuel capacity matches the fuel required for the design mission within a specified tolerance. The payload-range envelope of the resulting vehicle notionally resembles the envelope shown in Fig. 3(c). In this work, a combination of the secant method and the bi-section method is used to

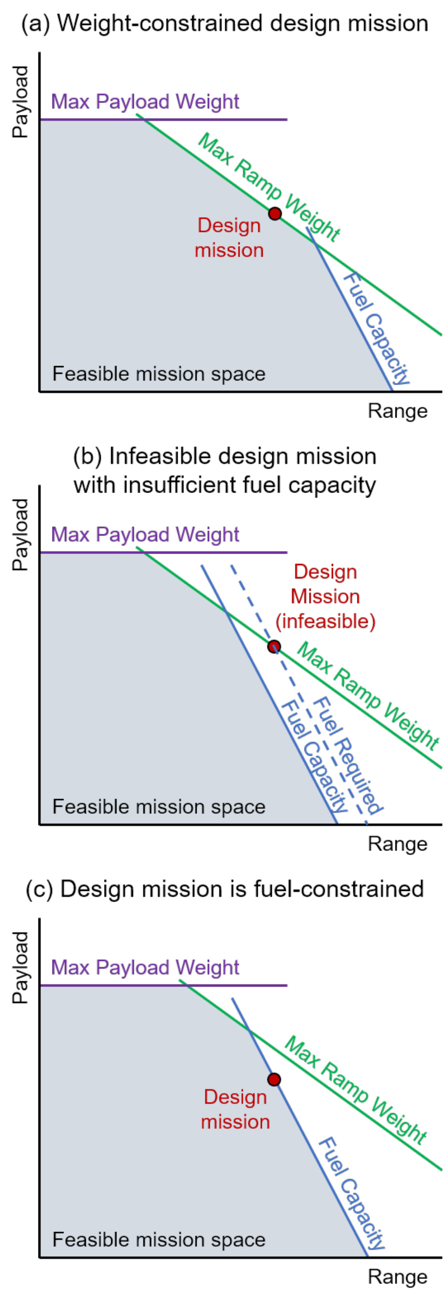

Figure 3: Notional payload-range diagrams for weight-constrained and fuel-constrained sizing

find the minimum feasible MRW in the case of fuel-constrained sizing.

4.3. Off-Design Mission Evaluation Scheme

The off-design mission evaluation involves determination of the payload-range envelope and the performance of off-design missions. Aircraft Sizing and Off-Design Mission Analyzer (SODA), a MATLAB program developed by the authors, automatically generates additional input data specifying the range, payload, and/or fuel available of each off-design mission, based on the output of the vehicle sizing module. In this work, a FLOPS interface is implemented in SODA, which translates the inputs to each off-design mission into relevant FLOPS namelists. SODA can be configured in six modes which evaluate three types of off-design missions, in addition to the design mission, as shown in Table 4 and Fig. 4. What follows is a concise description of the off-design evaluation modes.

Table 4: Mission evaluation modes in SODA

Mission Type	**Mode**					
	A	**B**	**C**	**D**	**E**	**F**
Design mission	✓	✓	✓	✓	✓	✓
Payload-range envelope		✓	✓	✓	✓	
Sample payload-range grid			✓		✓	
Specified off-design mission(s)				✓	✓	✓

4.3.1. Payload-Range Envelope

The payload-range envelope defines the boundary of the feasible mission space within which the aircraft is capable of flying for a given combination of payload and range. The envelope consists of three segments corresponding to three constraints:

1. **Maximum structural payload constraint.** The maximum structural

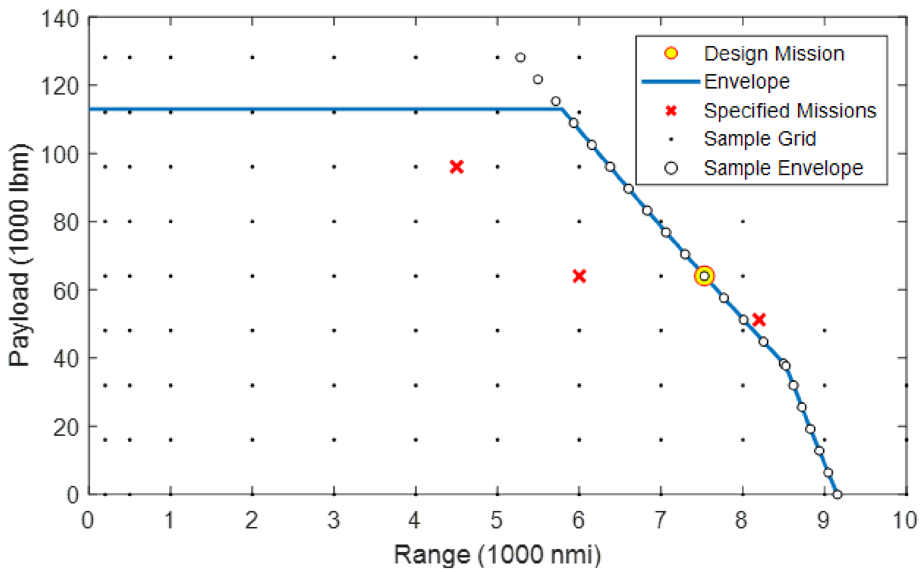

Figure 4: Notional payload-range diagram showing all mission types evaluated

payload weight (MPW) is the difference between the operating empty weight (OEW) and the maximum zero fuel weight (MZFW). MZFW and MPW are commonly used in detailed structural analysis, but not explicitly used for conceptual design in this work. Instead, MPW is estimated based on data for existing aircraft in the same size-class, and is assumed to remain constant for all design candidates in each size-class.

2. **Maximum ramp weight constraint.** The maximum ramp weight (MRW) is the maximum gross weight the aircraft can achieve when parked on the ground. In early design, the MRW is an important parameter used in sizing of major aircraft components, and specifically, in many component weight estimation equations in regression-based methods. The intersection of MRW and MPW constraints indicates the harmonic range, i.e. the maximum range the aircraft can reach when carrying full payload. It is assumed that MRW is the upper limit for gross weight when the aircraft starts a mission.

3. **Maximum fuel weight constraint.** The maximum fuel weight (MFW)

is the maximum amount of fuel which can be carried on-board. MFW is determined based on wing and fuselage geometry, and is used in fuel system sizing. The intersection of MRW and MFW constraints indicates the mission on which the aircraft departs at both MRW and MFW. It is assumed in this paper that MFW depends solely on the fuel capacity, while in reality, there may be weight and balance considerations which impose a more restrictive constraint on fuel allowed on-board based on allocation of payload even when the gross weight is smaller than MRW.

Since each candidate is constrained by the same design mission, the payload-range envelope always encloses the point representing the design mission in mission space. However, different design variables may result in different aerodynamic and propulsion characteristics and OEW, which affect the trade-off between payload and range, implied by different slopes of the MRW and MFW constraints. When assessing the impact on mission performance metrics of two candidates such as takeoff gross weight, block fuel, and PFEE, etc., comparison is valid only in the intersection of the two feasible mission spaces, i.e. the mission space containing missions that are common to both the candidates being compared.

4.3.2. Sample Grid

For a given aircraft, any mission performance metric strongly related to range and payload can be represented using a surrogate model [33, 34, 35] as shown in Eq. (9):

$$Q = h(W_p, R) \tag{9}$$

Examples of metric Q include takeoff gross weight, block fuel, and PFEE (Eq. (4)), etc. Once the mission space is sampled at multiple points, such surrogate modeling methods allow for fast evaluation of any off-design mission without actually running the physics-based mission analysis code. In addition, the surrogate models are also useful for creating contour plots and performing other assessments involving a large number of off-design mission evaluations.

To balance accuracy and execution time, the sample grid typically covers the interior of the envelope and extends beyond the envelope by a certain margin (as shown in Fig. 4), but can be user-defined for special cases.

4.3.3. Specified Missions

In order to eliminate model representation errors, off-design missions may be evaluated directly using true models (e.g. FLOPS) instead of using surrogate model(s). These missions are meant to represent payload-range combinations which are most commonly or typically flown by the aircraft. Without evaluating the envelope, the feasibility of each mission can be determined by comparing the payload weight, ramp weight, and mission fuel weight against MPW, MRW, and MFW from the sizing results.

4.4. Verification of the Analysis Environment

To verify the capability of SODA, a notional SSA is sized using the geometry and performance data as published in the Boeing 737-800 Airport Planning Document [36]. The resulting payload-range characteristics are compared in Fig. 5 and Table 5. It can be observed that, the payload-range envelope generated by SODA closely matches the reference envelope, and the off-design mission gross weights are within small errors from the reference values. Additionally, Fig. 5 also demonstrates SODA's capability to perform aircraft sizing using the fuel-constrained sizing algorithm as described in Sec. 4.3.

5. Optimization Algorithm

Most approaches that deal with multiple objectives solve a set of single-objective problems to compute the Pareto frontier [37, 38, 39]. Typically, in such approaches, a weighted aggregation of the objectives defines a single-objective problem. Multiple such instances with different weights are solved to obtain the complete Pareto frontier. Success of such methods relies on strong assumptions such as convexity of the frontier, among others. Moreover, the distribution of points obtained on the frontier heavily relies on the series of single-objective

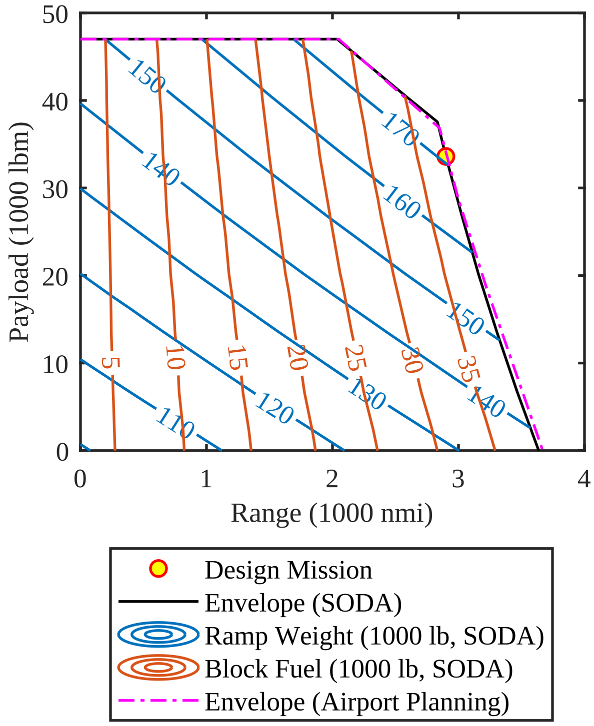

Figure 5: Comparison of payload-range characteristics between SODA outputs and Airport Planning data for a notional SSA resembling the Boeing 737-800

Table 5: Comparison of off-design mission gross weight computed by SODA and as published in the Airport Planning data for a notional SSA resembling the Boeing 737-800

Payload (lb)	**Range (lb)**	**Gross Weight (lb)**		**Error**
		SODA	**Reference**	
0	1500	113.8×10^3	112.7×10^3	+0.98 %
10 000	3000	142.6×10^3	142.0×10^3	+0.42 %
20 000	1000	130.8×10^3	129.2×10^3	+1.20 %
30 000	2500	161.0×10^3	160.5×10^3	+0.29 %
40 000	2000	166.1×10^3	165.7×10^3	+0.24 %

optimization problems solved. Therefore, in general, these methods are inappropriate candidates when an even distribution of points on the Pareto frontier is desired.

On the other hand, the NSGA-II [40, 41] operates on a population of designs (much like genetic algorithms) and successively refines it through metaheuristic operators like crossover, mutation, and selection until the members in the so-called evolved populations stop improving. The notion of improvement is handled through the concept of non-domination level. A member is said to be non-dominated when it is better than all the other members in the population in at least one objective. The NSGA-II converges by retaining the most non-dominated members which by definition lie on the Pareto frontier. In addition, the concept of non-domination level lends itself naturally to penalize members that violate constraints. In this paper, constraints are handled by artificially penalizing the non-domination level adversely to ensure that constraint violating designs get discarded as the algorithm progresses. It is known that in comparison to other algorithms that use gradient information, NSGA-II usually requires a higher number of function calls. However, a favorable feature of NSGA-II is that multiple designs can be evaluated simultaneously in parallel to alleviate the relatively higher computational costs it demands.

6. Results and Discussions

6.1. Sensitivity Analysis

A total of 12 000 samples are generated using the SALib [42] in Python and evaluated in SODA in MATLAB. The objective and constraint responses are extracted and analyzed via SALib's implementation of Sobol's method, which reports the individual effects of each design variable on each response. To conclude the sensitivity analysis, the design variables are ranked by their individual effects and then filtered by their cumulative effects on each objective and constraint response for each aircraft. The filtered effective design variables and their effects are summarized in Fig. 6. In this work, the threshold for normal-

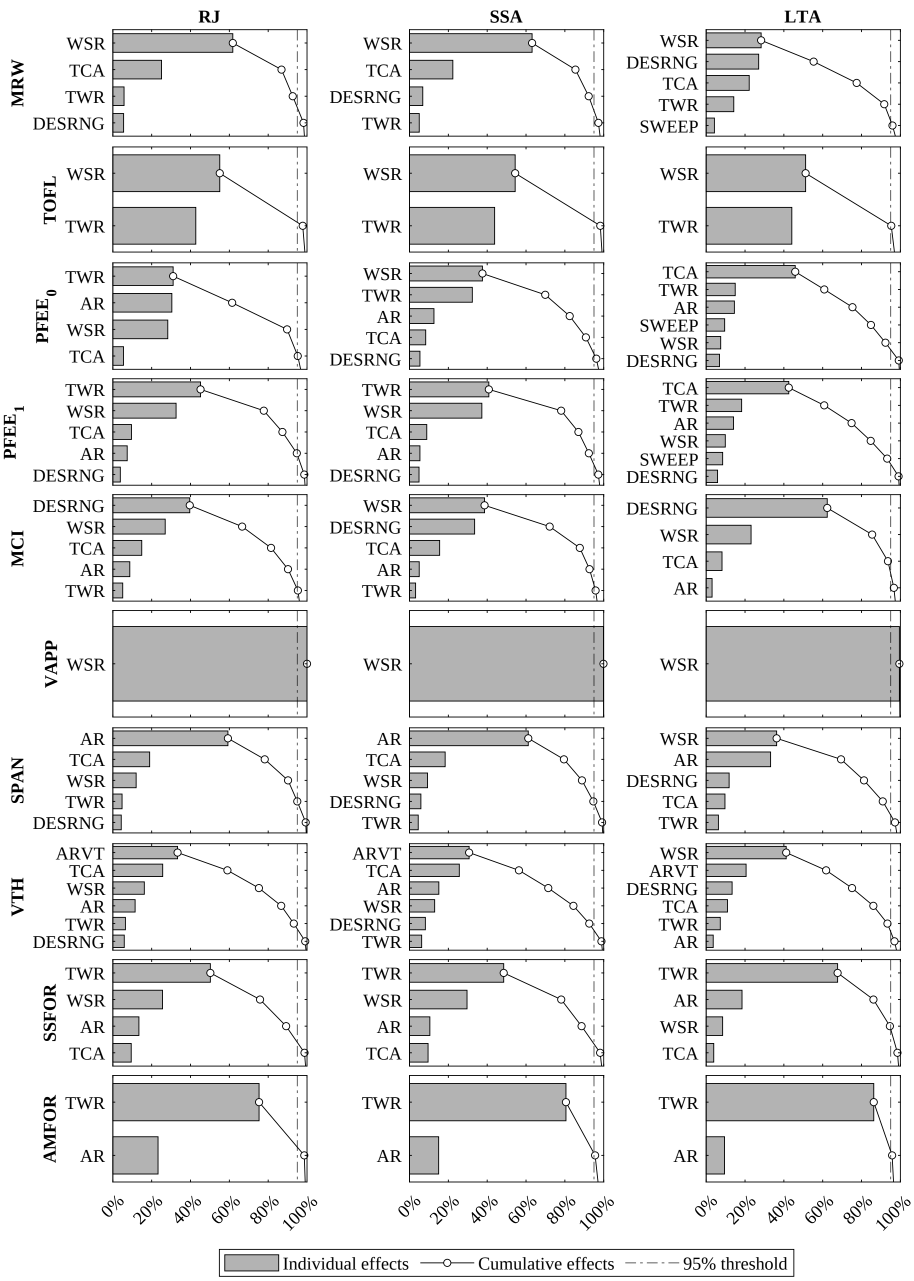

Figure 6: Normalized individual and cumulative effects of filtered effective design variables for individual responses

ized cumulative effects to determine the set of effective design variables is set to 95 %. Listed below in no particular order is the superset of all effective design variables for each response, members of which are used as the design variables for the optimization environment:

- TWR: sea-level static thrust-to-weight ratio
- WSR: design wing loading
- DESRNG: design range capability
- AR: wing aspect ratio
- TCA: wing average thickness-to-chord ratio
- SWEEP: wing quarter-chord sweep angle
- ARVT: vertical tail aspect ratio

As expected, observe that given the range of the design variables, the set of most effective design variables primarily include the vehicle-level parameters (TWR, WSR, and DESRNG) and wing geometry parameters (AR, TCA, and SWEEP). While ARVT does not have significant impact on any objective function, it has the most impact on the vertical tail height (VTH) which, as a constraint function, determines the design feasibility. Also note that the sensitivity depends on the range of the design variables and the design requirements which affect the function for each response. Therefore, the set of effective design variables may change based on the range of the design variables, the design requirements, and the selected threshold.

6.2. Summary of Optimization

The optimization environment is set up in MATLAB, with a wrapper transferring design variables and vehicle information to and from FLOPS. The MATLAB function `gamultiobj` is used to configure the NSGA-II algorithm. The population size is set to 150 for both on-design and off-design optimizations for each size-class. Some preliminary experiments indicate that these settings generate a sufficiently dense Pareto frontier while keeping the computational cost manageable. A scattered crossover function is used to form children arising from the crossover operator. The scattered crossover function selects members from the mating pool and randomly exchanges design variables between them to create off-springs for future generations. An adaptive feasible mutation function is used to randomly mutate selected individuals in directions and steps that are adapted based on the results in the past generations. As formulated in Sec. 2, a total of six optimization runs are performed, which are summarized in Table 6.

Table 6: Summary of the optimization runs for each aircraft

Case	**Population Size**	**Generations**	**Spread**
RJ, on-design	150	165	7.605×10^{-2}
RJ, off-design	150	102	6.283×10^{-2}
SSA, on-design	150	110	8.022×10^{-2}
SSA, off-design	150	119	8.061×10^{-2}
LTA, on-design	150	205	9.283×10^{-2}
LTA, off-design	150	150	6.925×10^{-2}

6.3. Comparison of Payload-Range Characteristics

Figure 7 presents a parallel coordinate plot for each size-class, showing the distribution of each design variable and objective of the final generation in both the on-design optimization and the off-design optimization, while highlighting the characteristics of the single-objective optimal designs. The bounds of each design variable (based on Table 1) are also marked in the plot, where for DESRNG, an artificial upper bound is placed at 110 % of the lower bound value for consistent axis scaling between the vehicles. Figure 8 presents the payload-range envelopes of the single-objective optimal designs overlaid on the off-design mission weighting function for each aircraft size-class. Since the mission weighting function is discrete and bounded on the payload-range plane, there exists no unique design that maximizes MCI; among all designs which maximize MCI, the one with the highest $PFEE_1$ is highlighted in Figs. 7 and 8.

6.3.1. Observations from On-Design Optimization

For all size-classes, in the on-design optimization, the mission weighting has no effect on the Pareto optimality. In this case, sizing for a higher range capability (DESRNG) than the required design range will cause an increase in the MRW. Therefore, the lower bound constraint on DESRNG is active for the entire population as seen in Fig. 7. In other words, the payload-range envelopes of all on-design optima pass through the design mission in each chart of Fig. 8.

For all on-design Pareto optima, the design mission is also always constrained by MRW for the entire population. As implied in Sec. 4.2, the fuel-constrained sizing algorithm requires upsizing the aircraft from the initial weight-constrained sizing output with all design variables held constant, which leads to an increase in MRW and fuel burn for all feasible missions, while not benefiting TOFL.

According to Fig. 7, the single-objective optimal designs for MRW and $PFEE_0$ have very similar performance, implying little trade-off between MRW and $PFEE_0$. It is also observed that, for these two designs, the design mission is both weight- and fuel-constrained as shown in Fig. 8, resulting in the worst mission capability (i.e. lowest MCI) among all Pareto optimal designs, as shown in Fig. 7.

6.3.2. Observations from Off-Design Optimization

In the off-design optimization, the mission weighting has an impact on the shape of payload-range envelope of Pareto-optimal designs: the shape of feasible mission space enclosed by the envelope affects both $PFEE_1$ and MCI by their definitions in Eqs. (6) and (7).

For the RJ, based on Fig. 8(a), a majority of the missions are within 1000 nmi while longer missions come with reduced payload. Therefore, weight-constrained designs with DESRNG at its lower bound, such as the optimal designs for MRW and $PFEE_0$ are already able to achieve high values for $PFEE_1$ and MCI, as

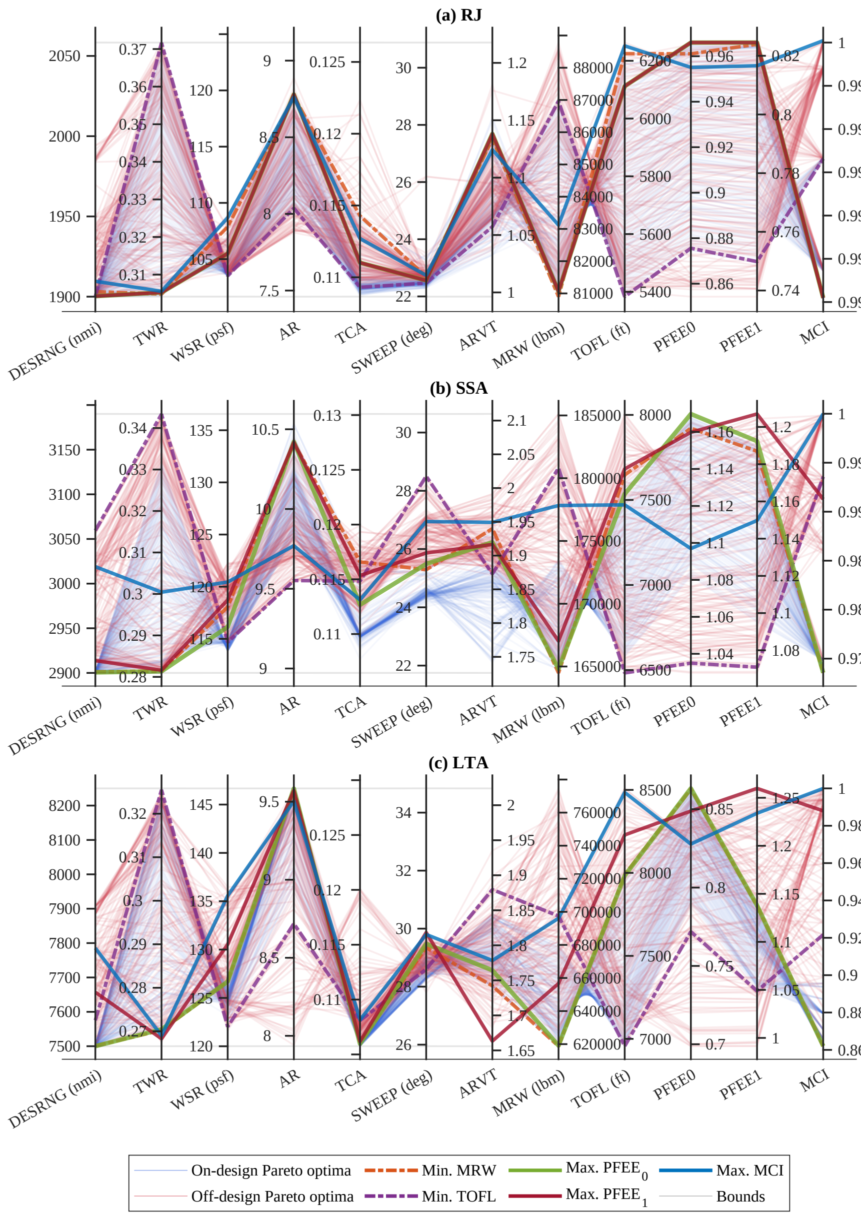

Figure 7: Design variables and objectives for Pareto optimal designs

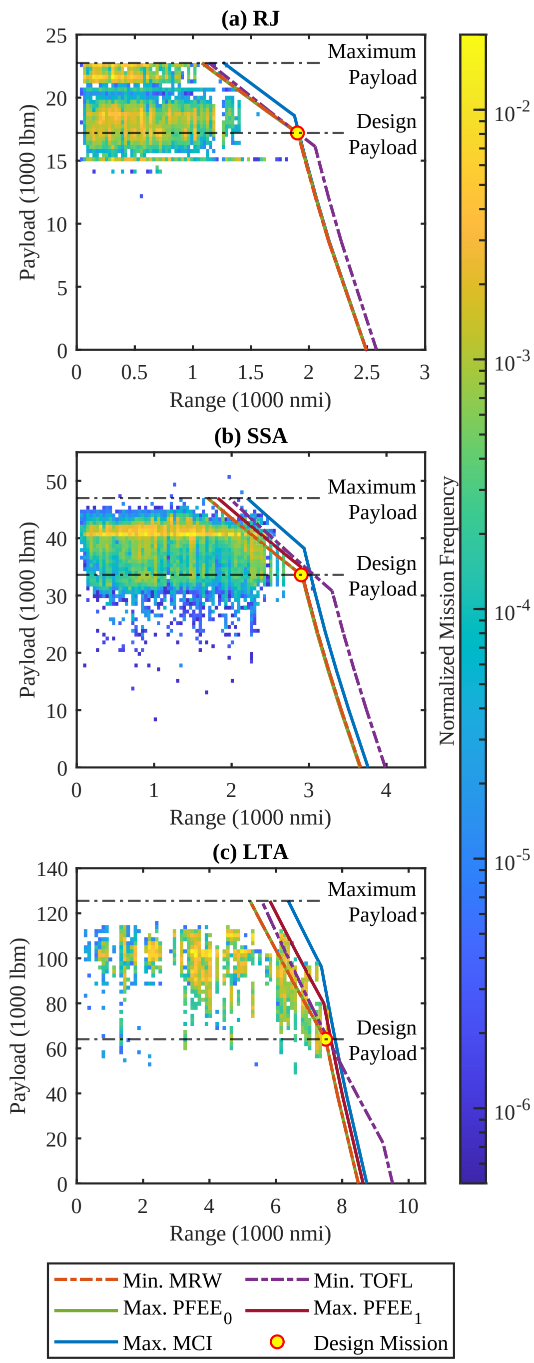

Figure 8: Payload-range envelopes of the single-objective optima

shown in Fig. 7(a). While it slightly improves MCI to further upsize the vehicle by increasing DESRNG and/or switching to fuel-constrained designs as indicated in Fig. 7(a), the marginal benefit of a higher mission coverage is negated by an overall increase in fuel consumption within the feasible mission space, thus worsening PFEE_1. Therefore, in the example of RJ, designs optimized for PFEE_0 and PFEE_1, respectively, have similar values for all performance metrics.

As the weighting function covers more missions in the long-and-heavy region on the payload-range plane, it may be necessary to upsize the vehicle to improve the flight productivity (PFEE_1) and mission capability (MCI).

In the examples of SSA and LTA, Figs. 7 and 8 show that the MCIs of the on-design Pareto optima are farther from 1 compared to that for the RJ, which makes PFEE_1 of the on-design optima sub-optimal. To achieve optimal PFEE_1, the off-design optimization attempts different values of the design variables. An increase in the design wing loading (WSR) as shown in Fig. 7(b)(c) reduces the wing area and the fuel capacity for a given MRW, thus triggering the fuel-constrained sizing algorithm to increase MRW to satisfy the fuel capacity constraint, as indicated by a rightward movement of the weight-constrained segment of the payload-range envelope in Fig. 8(b)(c). An increase in DESRNG may also be necessary to achieve optimal PFEE_1 by balancing the mission capability and fuel consumption. In the extreme case where MCI is maximized, the vehicle may be oversized for a noticeably longer range than the design range: according to Fig. 7(b) and (c), when optimized for MCI, both SSA and LTA are sized for a range of approximately 4 % longer than the required design range, at the cost of significantly larger MRW and smaller PFEE_1.

6.4. Comparison of Objectives and Pareto Frontiers

The scatterplot matrices in Figs. 9 through 11 plot the MRW, TOFL, PFEE_0, PFEE_1, and MCI of the final population in both on-design and off-design optimization for each aircraft size-class, where the arrow in each cell indicates the direction of improvement on each projection plane.

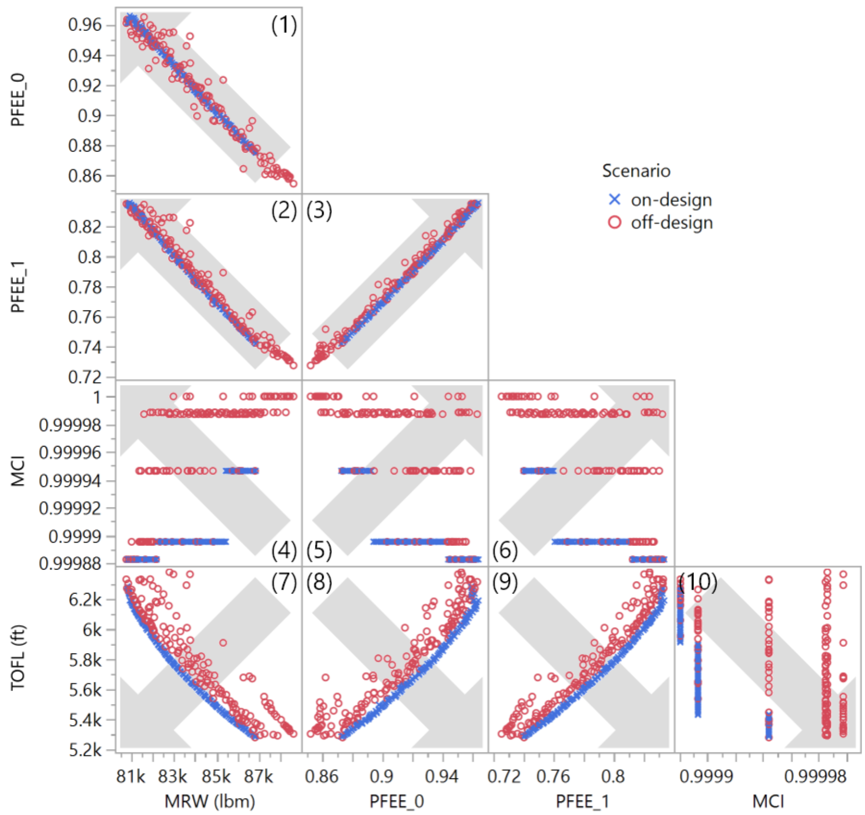

Figure 9: Projected Pareto frontiers for RJ

6.4.1. *Observations from On-Design Optimization*

For each size-class, in the on-design optimization, the Pareto frontier appears to be a curve in the three-dimensional space formed by MRW, TOFL, and $PFEE_0$. When considering only two objectives at a time, the projected on-design 3-D Pareto frontier in subplots (7) and (8) form 2-D Pareto frontiers for MRW vs TOFL and $PFEE_0$ vs TOFL, while in subplot (1), MRW and $PFEE_0$ simultaneously reach their optimal values. Note that, based on the definition in Eq. (5), $PFEE_0$ is only related to the design mission block fuel. The results are therefore consistent with the positive correlation between gross weight and fuel consumption for a given mission. This also explains why the design mission, the only mission that concerns the on-design optimization, is always weight-

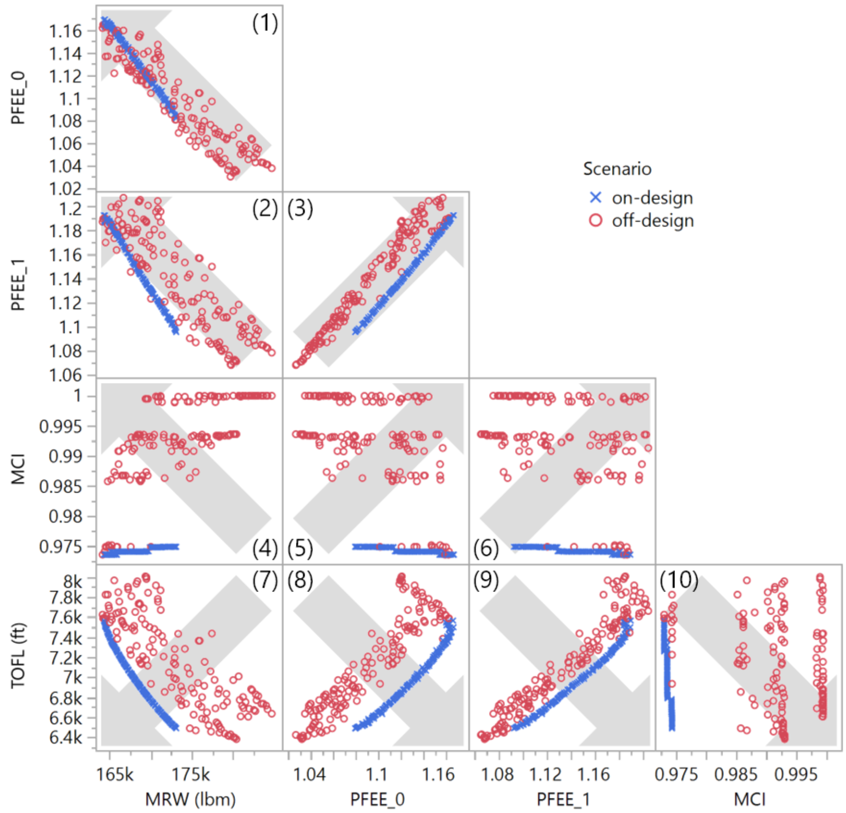

Figure 10: Projected Pareto frontiers for SSA

constrained for the entire Pareto optimal population.

On the other hand, the goal to minimize TOFL conflicts with minimizing MRW and maximizing PFEE_0 (i.e. minimizing design mission block fuel), since a shorter TOFL requires more powerful engines for the same take-off gross weight, which translates to a higher TWR (as shown in Fig. 7) and in turn increases the size of engines and fuel flow at cruise, resulting in higher fuel consumption and MRW.

6.4.2. Observations from Off-Design Optimization

For the RJ, given the mission weighting function focusing on short missions, the off-design Pareto frontier is generally aligned with the on-design Pareto fron-

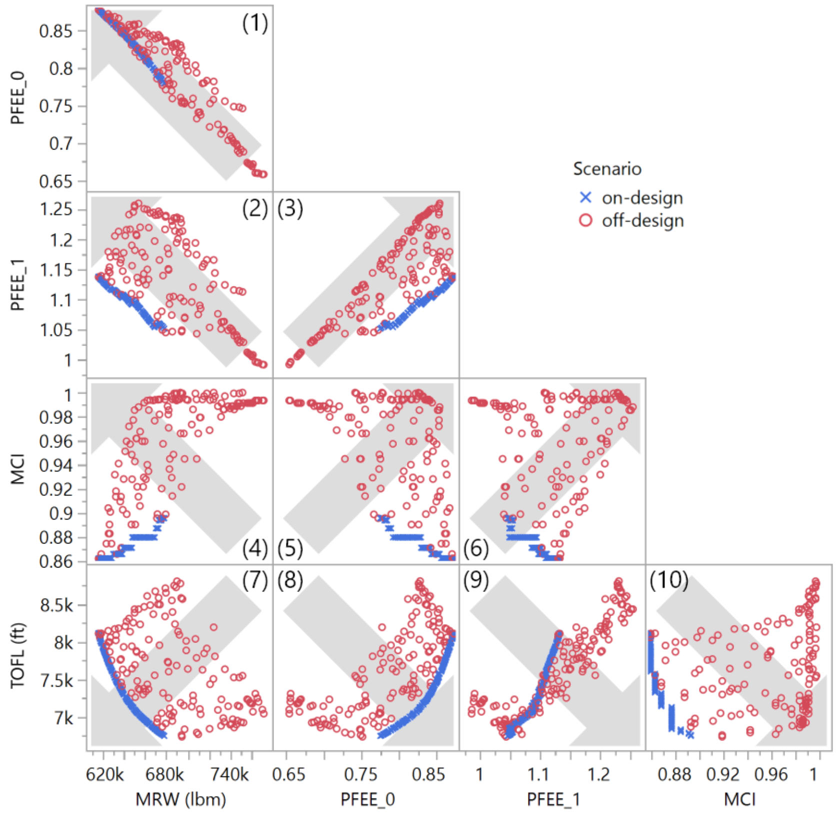

Figure 11: Projected Pareto frontiers for LTA

tier. As discussed in Sec. 6.3, there is no motivation to trade MRW for PFEE_1, therefore MRW and PFEE_1 can reach their optimal values simultaneously as shown in Fig. 9 subplot (2). When comparing on-design and off-design optimization, the patterns of the projected PFEE_0 vs PFEE_1 values in subplot (3) clearly align with each other, indicating that the Pareto optimal designs have similar values for the pair PFEE_0 and PFEE_1 regardless of the goal of optimization.

For the SSA, Fig. 10 subplot (2) implies a trade-off between MRW and PFEE_1 when considering these two objectives only, as discussed in Sec. 6.3.2. Note that the Pareto frontier of MRW vs PFEE_1 in subplot (2) only spans over a smaller interval of MRW compared to the Pareto frontier of MRW vs TOFL in subplot (7). The reason is that, as MRW increases beyond a certain threshold (approximately 167×10^3 lbm in this case), the disadvantage of higher fuel consumption offsets the benefit gained by covering more missions, resulting in a decrease in PFEE_1 from the single-objective maximum; this is consistent with the discussions made in Sec. 6.3.2. In subplot (3), towards higher PFEE_0 values, a few designs optimized for off-design missions interestingly appear superior than the on-design candidates optimized for the same PFEE_0 value, indicating a marked benefit in productivity over a purely on-design performance centric design optimization. This observation clearly highlights the benefit in optimizing for off-design performance (or productivity as indicated by PFEE_1).

For the LTA, as shown in Fig. 11, the trade-off between MRW and PFEE_1 is even more significant in subplot (2), where the single-objective maximum value of PFEE_1 is approximately 11 % greater than the PFEE_1 value for the minimum-MRW design. The wide-spread pattern of the off-design Pareto optima above the on-design Pareto optima in subplot (3) implies that designs optimized merely for the design mission may be suboptimal in actual airline operations than the designs optimized for the given off-design missions. Also note that the PFEE_0 value of the single-objective optimum design for PFEE_1 is approximately 2.1 % lower than the maximum value of PFEE_0, indicating a trade-off between PFEE_0 and PFEE_1.

7. Conclusion

This paper presents a multi-objective constrained optimization approach for aircraft sizing, taking into account both on-design and off-design mission performance metrics. Parsimonious optimization problems are formulated by down-selecting inputs from a large set of design variables that captured most of the variance in the objective and constraint functions. An off-design mission weighting function is used to transform mission-dependent variables such as payload, range, fuel consumption into a scalar through an integration on the feasible mission space identified by the payload-range envelope of a sized vehicle. In this work, historical mission data are used to obtain the mission weighting function for each vehicle size-class being studied, which simulates the market in which a new design of the same size-class is expected to operate. Results show that the mission weighting function has a strong impact on the Pareto optimal designs when off-design mission performance metrics such as the payload fuel energy efficiency and the mission coverage index are explicitly considered as objectives along with mission-invariant characteristics such as the maximum ramp weight and maximum takeoff field length at standard sea-level condition. When the long-and-heavy missions are given higher weighting, increasing the design range capability and/or switching to fuel-constrained sizing modifies the shape of payload-range envelope and may increase the flight productivity with a penalty on the maximum ramp weight, as shown in the examples of the Small Single-aisle Aircraft and the Large Twin-aisle Aircraft.

Some avenues for future work include: 1) employ more accurate aerodynamics, weights, and propulsion system analysis, which still exploit high-level vehicle design parameters to obtain better estimation of vehicle performance metrics; 2) consider the impact of subsystem architectures which may impact vehicle empty weight, fuel burn, and drag characteristics in different manners; 3) consider and quantify the impact of different choices of mission weighting function and mission-dependent metrics on the Pareto optimal solutions; 4) establish a process which facilitates making decisions regarding whether a family of aircraft (instead of a single type) should be designed to split the market share in order to improve flight productivity given the set of Pareto optimal designs based on the selected metrics and mission weighting function.

References

[1] RoutesOnline, Singapore airlines a340-500 routes: 2004 – 2013, Online (Nov. 2013).
URL `https://www.routesonline.com/news/29/breaking-news/166752/singapore-airlines-to-close-los-angeles-and-newark-routes/`

[2] R. P. Liem, Multimission Fuel-Burn Minimization in Aircraft Design: A

Surrogate-Modeling Approach, University of Toronto (Canada), 2015.
URL https://www.proquest.com/docview/1719288320

[3] R. P. Liem, G. K. W. Kenway, J. R. R. A. Martins, Multimission aircraft fuel-burn minimization via multipoint aerostructural optimization, AIAA Journal 53 (1) (2015) 104–122. doi:10.2514/1.j052940.

[4] D. M. Straussfogel, Formulation of the multimission aircraft design optimization problem, Ph.D. thesis, The Pennsylvania State University (1998).
URL https://search.proquest.com/docview/304443893

[5] B. M. Yutko, The impact of aircraft design reference mission on fuel efficiency in the air transportation system, Ph.D. thesis, Massachusetts Institute of Technology (2013).
URL https://dspace.mit.edu/handle/1721.1/87482

[6] X. CHAI, X. YU, Y. WANG, Multipoint optimization on fuel efficiency in conceptual design of wide-body aircraft, Chinese Journal of Aeronautics 31 (1) (2018) 99–106. doi:10.1016/j.cja.2017.10.006.

[7] M. J. Daskilewicz, B. J. German, T. T. Takahashi, S. Donovan, A. Shajanian, Effects of disciplinary uncertainty on multi-objective optimization in aircraft conceptual design, Structural and Multidisciplinary Optimization 44 (6) (2011) 831–846. doi:10.1007/s00158-011-0673-4.
URL https://doi.org/10.1007/s00158-011-0673-4

[8] D. Rajaram, Y. Cai, I. Chakraborty, D. N. Mavris, Integrated sizing and optimization of aircraft and subsystem architectures in early design, Journal of Aircraft 55 (5) (2018) 1942–1954. doi:10.2514/1.c034661.

[9] H. Jimenez, D. Mavris, Pareto-optimal aircraft technology study for environmental benefits with multi-objective optimization, Journal of Aircraft 54 (5) (2017) 1860–1876. doi:10.2514/1.c033688.

[10] D. Rajaram, Y. Cai, I. Chakraborty, T. G. Puranik, D. N. Mavris, Integrated sizing and multi-objective optimization of aircraft and subsystem

architectures in early design, in: 17th AIAA Aviation Technology, Integration, and Operations Conference, 2017, p. 3067.

[11] P.-J. Proesmans, R. Vos, Airplane design optimization for minimal global warming impact, in: AIAA Scitech 2021 Forum, American Institute of Aeronautics and Astronautics, 2021. doi:10.2514/6.2021-1297.

[12] J. Hileman, J. Katz, J. Mantilla, G. Fleming, Payload fuel energy efficiency as a metric for aviation environmental performance, ICAS Secretariat - 26th Congress of International Council of the Aeronautical Sciences 2008, ICAS 2008 2 (2008) 3314–3324.

[13] Aviation fuel – jet a/jet a-1 (2019).
URL https://www.exxonmobil.com/en/aviation/products-and-services/products/jet-a-jet-a-1

[14] S. Patnaik, R. Coroneos, J. Guptill, D. Hopkins, W. Haller, A subsonic aircraft design optimization with neural network and regression approximators, in: 10th AIAA/ISSMO Multidisciplinary Analysis and Optimization Conference, American Institute of Aeronautics and Astronautics, 2004. doi:10.2514/6.2004-4606.

[15] Advisory circular ac 150/5300-13a, Online (Feb. 2014).
URL https://www.faa.gov/documentLibrary/media/Advisory_Circular/150-5300-13A-chg1-interactive-201907.pdf

[16] J. D. Mattingly, W. H. Heiser, D. T. Pratt, Aircraft Engine Design, Second Edition, American Institute of Aeronautics and Astronautics, 2002. doi:10.2514/4.861444.

[17] S. Shan, G. G. Wang, Survey of modeling and optimization strategies to solve high-dimensional design problems with computationally-expensive black-box functions, Structural and Multidisciplinary Optimization 41 (2) (2010) 219–241. doi:10.1007/s00158-009-0420-2.
URL http://link.springer.com/10.1007/s00158-009-0420-2

[18] S. Shan, G. G. Wang, Metamodeling for High Dimensional Simulation-Based Design Problems, Journal of Mechanical Design 132 (5) (2010) 051009. `doi:10.1115/1.4001597`.
URL `http://mechanicaldesign.asmedigitalcollection.asme.org/article.aspx?articleid=1450036`

[19] R. H. Myers, D. C. Montgomery, C. M. Anderson-Cook, Response surface methodology : process and product optimization using designed experiments., Wiley, 2009.

[20] I. M. Sobol, Global sensitivity indices for nonlinear mathematical models and their monte carlo estimates, Mathematics and computers in simulation 55 (1-3) (2001) 271–280. `doi:10.1016/S0378-4754(00)00270-6`.
URL `https://doi.org/10.1016/S0378-4754(00)00270-6`

[21] A. Saltelli, Making best use of model evaluations to compute sensitivity indices, Computer physics communications 145 (2) (2002) 280–297. `doi:10.1016/S0010-4655(02)00280-1`.
URL `https://doi.org/10.1016/S0010-4655(02)00280-1`

[22] Air carrier statistics (form 41 traffic)- u.s. carriers, Online (Oct. 2018).
URL `https://www.transtats.bts.gov/tables.asp?db_id=110&DB_Name=`

[23] D. Brain, N. Voorbach, Icao's global horizontal flight efficiency analysis, resreport, International Civil Aviation Organization (2019).
URL `https://www.icao.int/environmental-protection/Documents/EnvironmentalReports/2019/ENVReport2019_pg138-144.pdf`

[24] D. N. Mavris, Classical design methods, Lecture Notes (Aug. 2016).

[25] L. McCullers, Flight Optimization System, Release 8.11, User's Guide, NASA Langley Research Center, Hampton, VA 23681-0001 (Oct. 2009).

[26] B. L. Horvath, D. P. Wells, Comparison of aircraft conceptual design weight estimation methods to the flight optimization system, in: 2018 AIAA

Aerospace Sciences Meeting, American Institute of Aeronautics and Astronautics, 2018. doi:10.2514/6.2018-2032.

[27] D. Raymer, Aircraft Design: A Conceptual Approach, Fifth Edition, American Institute of Aeronautics and Astronautics, Inc., 2012. doi:10.2514/4.869112.

[28] D. J. Roskam, Airplane Design Part V: Component Weight Estimation, Design, Analysis and Research Corporation (DARcorporation), 1999.

[29] D. P. Wells, B. L. Horvath, L. A. McCullers, The flight optimization system weights estimation method (2017).

[30] J. Lytle, G. Follen, C. Naiman, A. Evans, Numerical propulsion system simulation (npss) 1999 industry review (2000).

[31] M. T. Tong, B. A. Naylor, An object-oriented computer code for aircraft engine weight estimation, in: Volume 1: Aircraft Engine; Ceramics; Coal, Biomass and Alternative Fuels; Manufacturing, Materials and Metallurgy; Microturbines and Small Turbomachinery, ASME, 2008. doi:10.1115/gt2008-50062.

[32] I. Annex, Rules of the air (Jul. 2005).
URL https://www.icao.int/Meetings/anconf12/Document%20Archive/an02_cons%5B1%5D.pdf

[33] R. P. Liem, C. A. Mader, J. R. Martins, Surrogate models and mixtures of experts in aerodynamic performance prediction for aircraft mission analysis, Aerospace Science and Technology 43 (2015) 126–151. doi:10.1016/j.ast.2015.02.019.
URL https://doi.org/10.1016/j.ast.2015.02.019

[34] J. Yanto, R. P. Liem, Aircraft fuel burn performance study: A data-enhanced modeling approach, Transportation Research Part D: Transport and Environment 65 (2018) 574–595. doi:10.1016/j.trd.2018.09.014.
URL https://doi.org/10.1016/j.trd.2018.09.014

[35] Y. Lyu, R. P. Liem, Flight performance analysis with data-driven mission parameterization: mapping flight operational data to aircraft performance analysis, Transportation Engineering 2 (2020) 100035. doi:10.1016/j.treng.2020.100035.
URL https://doi.org/10.1016/j.treng.2020.100035

[36] Boeing Commercial Airplanes, 737 Airplane Characteristics for Airport Planning (Sep. 2013).
URL https://www.boeing.com/resources/boeingdotcom/commercial/airports/acaps/737.pdf

[37] J. Sanchis, M. Martinez, X. Blasco, J. Salcedo, A new perspective on multi-objective optimization by enhanced normalized normal constraint method, Structural and multidisciplinary optimization 36 (5) (2008) 537–546.

[38] A. Messac, A. Ismail-Yahaya, C. A. Mattson, The normalized normal constraint method for generating the pareto frontier, Structural and multidisciplinary optimization 25 (2) (2003) 86–98.

[39] I. Das, J. E. Dennis, Normal-boundary intersection: A new method for generating the pareto surface in nonlinear multicriteria optimization problems, SIAM Journal on Optimization 8 (3) (1998) 631–657.

[40] K. Deb, A. Pratap, S. Agarwal, T. Meyarivan, A fast and elitist multi-objective genetic algorithm: Nsga-ii, IEEE transactions on evolutionary computation 6 (2) (2002) 182–197.

[41] K. Deb, Multi-objective optimization using evolutionary algorithms, Vol. 16, John Wiley & Sons, 2001.

[42] J. Herman, W. Usher, SALib: An open-source python library for sensitivity analysis, The Journal of Open Source Software 2 (9) (jan 2017). doi:10.21105/joss.00097.
URL https://doi.org/10.21105/joss.00097